Proceedings of the ASME 2018 Dynamic Systems and Control Conference
DSCC 2018
Sept 30-Oct 3, 2018, Atlanta, USA

DSCC2018-9079

A DYNAMICS-AGNOSTIC STATE ESTIMATOR FOR UNMANNED AERIAL VEHICLES USING ULTRA-WIDEBAND RADIOS

Mark W. Mueller
Department of Mechanical Engineering
University of California
Berkeley, California 94720
Email: mwm@berkeley.edu

ABSTRACT

We present a state estimator for a UAV operating in an environment equipped with ultra-wideband radio beacons. The beacons allow the UAV to measure distances to known positions in the world. The estimator additionally uses the vehicle's rate gyroscope and accelerometer, and crucially does not rely on any knowledge of the vehicle's dynamic properties (e.g. mass, mass moment of inertia, aerodynamic properties). This makes the estimator especially useful in situations where the exact system parameters are unknown (e.g. due to unknown payloads), or where the environment is unpredictable (e.g. wind gusts). Experimental results demonstrate the approach's efficacy, and demonstrate that the estimator can run on low-cost microcontrollers with typical sensors.

INTRODUCTION

Unmanned Aerial Vehicles (UAVs) are rapidly expanding their capabilities. These systems have already found wide-spread acceptance as hobbies and toys, and continuing improvements and modernization of legal standards has allowed their commercial use to increase as well. Their low cost and versatility make them particularly attractive for applications such as remote sensing, monitoring, and surveillance, especially in environments where human access is difficult, or where conditions that expose human operators to danger.

A primary cost driver for current UAV systems is the typical requirement of a human operator to pilot the vehicle. Reducing the reliance on an expert human operator promises to further reduce the cost of operations. Such autonomy, however, requires that the UAV is able to localize itself (either absolutely, or relative to objects of interest such as infrastructure to be inspected).

Many different approaches exist for object localization. Most well-known are approaches that rely on satellite navigation systems, such as the GPS constellation. These provide global positioning, with reasonable accuracy, but are only useable if the vehicle has an unobstructed view of the satellites, so that such systems are not applicable to indoor operations, or operations near large structures that may occlude part of the sky. A popular approach in research laboratories uses motion capture systems (originally developed for motion digitization), as in, for example, [1–4]. These systems are attractive because they provide very high-quality data: typically measurements are taken at rates above 100Hz, and the measurements include the objects' position and orientation (with typical precision at or below 1mm/1°). Such systems, however, are extremely restricted in application, as they are expensive, require unobstructed views, and typically are only capable of measuring a relatively small volume.

A popular research topic is to use cameras mounted on the vehicles, performing some form of simultaneous localization and mapping (SLAM) [5]; examples include [6–10]. Such systems are attractive as they do not rely on any external infrastructure, and all sensors are fully contained on the vehicle. However, they do require very large computational resources, and tend to be fragile (struggling, for example, with changes in light or environments with poor visibility).

Yet another approach uses ultra-wideband radios for localization. This radio technology uses very wide bandwidth radio transmissions coupled with accurate clocks to measure distance through signal time of flight (see e.g. [11–14]). This approach has the advantage of relying on relatively inexpensive hardware, and may be robust to external interference, poor environmental conditions (e.g. low visibility) etc., but provides only relatively sparse localization data.

In this paper we build on prior work [14], by developing a system allowing a mutlicopter to fly autonomously using a set of ultra-wideband beacons and inertial sensors. However, compared to [14], we use an improved formulation for statistical correctness [15], and crucially make no assumptions about the vehicle's dynamic properties for the estimator. Specifically, we do not assume any knowledge of the vehicle's inertial parameters, nor of its aerodynamic properties. Thus, the resulting estimator is more robust, and may be straight-forwardly applied in situations where the vehicle's physical parameters are unknown (e.g. when carrying loads) or when the environment contains substantial wind effects.

This paper is organized as follows: we briefly recapitulate multicopter dynamics, in the next section; then we develop the state estimator that will be used. Experimental validation is provided next, followed by a conclusion.

SYSTEM DYNAMICS AND ARCHITECTURE

This section provides a brief introduction to the dynamics of a quadcopter, and the radio beacon system used. It introduces the relevant system states and their differential equations. The dynamics will be derived specifically for a quadcopter UAV, however the estimator may be applied to UAVs with other dynamics without modification.

In the agent's environment, a set of radio beacons are placed at known locations, where $\underline{b}_i$ indicates the position of beacon i. It is assumed that the beacons are well-spread through the area of interest.

A typical UAV can be well modeled as a rigid body with six degrees of freedom. We denote its position relative to some fixed point as $\underline{p} \in \mathbb{R}^3$ (expressed in an inertial coordinate system), and its velocity and acceleration as $\underline{v}$ and $\underline{a}$ (expressed in the same inertial coordinate system) so that

$$\underline{v} = \frac{\mathrm{d}}{\mathrm{d}t}\underline{p} \tag{1}$$

$$\underline{a} = \frac{\mathrm{d}}{\mathrm{d}t}\underline{v} \tag{2}$$

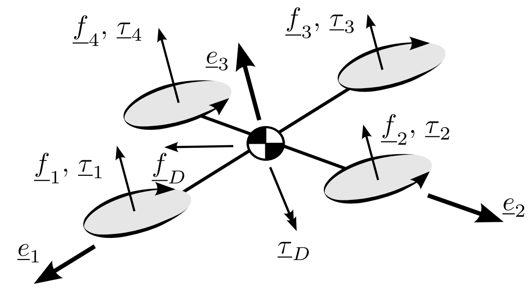

FIGURE 1. DYNAMIC MODEL OF A QUADCOPTER.

The body's orientation with respect to the inertial frame is captured by the rotation matrix $\underline{R} \in \mathrm{SO}(3)$, so that a vector $\underline{a_b}$ expressed in the body-fixed frame is transformed to the inertial coordinate system $\underline{a_i}$ by

$$\underline{a_i} = \underline{R}\underline{a_b} \tag{3}$$

The rotation matrix evolves as a function of the angular velocity $\underline{\omega} \in \mathbb{R}^3$ and angular acceleration $\underline{\alpha}$ (both expressed in the body-fixed frame).

$$\frac{\mathrm{d}}{\mathrm{d}t}\underline{R} = \underline{R}\,S(\underline{\omega}) \tag{4}$$

$$\frac{\mathrm{d}}{\mathrm{d}t}\underline{\omega} = \underline{\alpha} \tag{5}$$

where $S(\cdot) : \mathbb{R}^3 \to \mathrm{so}(3)$ produces the skew-symmetric matrix form of the vector argument (often called the "hat-map"), specifically if $\underline{x} = (x_1, x_2, x_3)$ then

$$S(\underline{x}) = \begin{bmatrix} 0 & -x_3 & x_2 \\ x_3 & 0 & -x_1 \\ -x_2 & x_1 & 0 \end{bmatrix} \tag{6}$$

The translational and angular accelerations can be related to external forces and torques acting on the system through the Newton-Euler equations [16], below. The vehicle's mass is denoted m, its mass moment of inertia (expressed in body-fixed) as the matrix $\underline{J}$, the forces (excluding weight due to gravity $\underline{g}$) acting on the vehicle (expressed in inertial) as $\underline{f_\Sigma}$, and the external torques acting on the vehicle as $\underline{\tau_\Sigma}$ (expressed in body-fixed).

$$\underline{a} = \frac{1}{m}\underline{f_\Sigma} + \underline{g}. \tag{7}$$

$$\underline{\alpha} = \underline{J}^{-1}\left(\underline{\tau_\Sigma} - S(\underline{\omega})\,\underline{J}\underline{\omega}\right) \tag{8}$$

The forces acting on the system $\underline{f_\Sigma}$ can be broken into the four forces produced by the propellers ($\underline{f_i}$) and all other forces $\underline{f_D}$ (typically considered disturbances when controlling the vehicle). The forces produced by the propellers are typically well known, as this knowledge is crucial for successful control of the UAV. However, the disturbance forces $\underline{f_D}$ are much harder to characterize. Disturbances may include aerodynamic effects (see e.g. [14, 17–20]) as well as other effects due to e.g. misaligned actuators. Likewise, the total moment is composed of the moments produced by the propellers (both around their axes of rotation as well as the force acting at a distance from the center of mass) and other disturbance moments. These disturbance moments may be due to aerodynamics, actuator mismodelling, etc.

ESTIMATOR

The output of the estimator is an estimate of the vehicle's position, velocity, orientation, and angular velocity. The estimator is an extended Kalman filter, following the method of [15] to encode uncertainty in the vehicle's attitude.

Prediction model

The estimator's prediction model uses the equations (1), (2), and (5). Notably, the estimator does not use the Newton-Euler dynamics equations, as these require knowledge of the vehicle's inertial properties as well as external forces and torques. Instead, the estimator uses the vehicle's inertial measurement unit (accelerometer and rate gyroscope) in the prediction step. Symbols with a tilde denote measurements, and specifically the accelerometer measurement $\underline{\widetilde{m_a}}$ is related to the vehicle's acceleration $\underline{a}$ as

$$\underline{\widetilde{m_a}} = \underline{R}^{-1}\left(\underline{a} - \underline{g}\right) + \underline{\nu}_{m_a} \tag{9}$$

where $\underline{\nu}_{m_a}$ is the sensor noise, and we make the assumption that the accelerometer is located at the vehicle's center of mass, through which the instantaneous axis of rotation is furthermore assumed to pass. This means that the accelerometer measurement is independent of the vehicle's angular dynamics.

The rate gyroscope measurement is given by

$$\underline{\widetilde{m_\omega}} = \underline{\omega} + \underline{\nu}_{m_\omega} \tag{10}$$

with $\underline{\nu}_{m_\omega}$ the sensor noise.

From this follows

$$\underline{a} = \underline{R}\underline{\widetilde{m_a}} + \underline{g} - \underline{R}\underline{\nu}_{m_a} \tag{11}$$

$$\underline{\omega} = \underline{\widetilde{m_\omega}} - \underline{\nu}_{m_\omega} \tag{12}$$

which may now be used in the prediction model.

Both the accelerometer and rate gyroscope are assumed to output regular measurements at a high frequency.

Measurement model

The ultra-wideband radio measures the distance $\widetilde{r}_i$ from the agent to radio beacon i, as

$$\widetilde{r}_i = \left\|\underline{p} - \underline{b}_i\right\| + \nu_r \tag{13}$$

where $\|\cdot\|$ indicates the 2-norm, and ν_r is sensor noise.

The ultra-wideband radios require a set of four radio messages to be communicated between the agent and the beacon for a single distance measure. As each measurement is subject to interference, these measurements are available only irregularly, with a relatively low frequency compared to the inertial sensors. Furthermore, at any particular time instance, the distance to at most one radio beacon can be measured.

EKF implementation

We implement an extended Kalman filter (EKF) with a nine-dimensional state vector, according to the method of [15]. This state vector consists of the vehicle position $\underline{\hat{p}}$, velocity $\underline{\hat{v}}$, and a three-dimensional representation of the attitude error $\underline{\hat{\delta}}$, and a reference orientation $\underline{\hat{R}_{\text{ref}}}$. The resulting attitude error is then computed as

$$\underline{\hat{R}} = \underline{\hat{R}_{\text{ref}}} \exp\left(S\left(\underline{\hat{\delta}}\right)\right) \tag{14}$$

with $\exp(\cdot)$ the matrix exponential so that $\exp(S(\cdot))$ returns a rotation matrix [21].

The estimator state vector is given by $\hat{x} = \left(\underline{\hat{p}}, \underline{\hat{v}}, \underline{\hat{\delta}}\right) \in \mathbb{R}^9$ and is predicted forward in time according to the difference equation

$$\hat{x}_p(t+\Delta t) = \hat{x}(t) + \begin{bmatrix} \frac{\mathrm{d}}{\mathrm{d}t}\underline{\hat{p}}(t) \\ \frac{\mathrm{d}}{\mathrm{d}t}\underline{\hat{v}}(t) \\ \frac{\mathrm{d}}{\mathrm{d}t}\underline{\hat{\delta}}(t) \end{bmatrix} \Delta t$$

$$= \begin{bmatrix} \underline{\hat{p}}(t) + \underline{\hat{v}}(t)\Delta t \\ \underline{\hat{v}} + \left(\left(\underline{\hat{R}_{\mathrm{ref}}}(t) \exp\left(S\left(\underline{\hat{\delta}}(t) \right) \right) \right)^{-1} \underline{\widetilde{m_a}}(t) + \underline{g} \right) \Delta t \\ \delta(t) + \left(\underline{\widetilde{m_\omega}}(t) - \frac{1}{2} S\left(\underline{\widetilde{m_\omega}}(t) \right) \delta(t) \right) \Delta t \end{bmatrix} \tag{15}$$

wherein the IMU data are taken as constant over the sampling time Δt. The differential equation for the attitude error is valid only because the attitude error is set to zero after each step (by updating the reference attitude and covariance matrix). It is important to notice that (15) requires no physical parameters of the vehicle, and in fact contains nothing specific to the quadcopter dynamics.

The estimated variance matrix $P_{xx} \in \mathbb{R}^{9\times 9}$ is predicted forward in time using the standard EKF equations

$$P_{xx,p}(t+\Delta t) = A(t) P_{xx}(t) A(t)^T + Q \tag{16}$$

where

$$A(t) = \begin{bmatrix} I & I\Delta t & 0 \\ 0 & I & S\left(\underline{\hat{R}_{\mathrm{ref}}}(t)^{-1} \underline{\widetilde{m_a}}(t) \right) \Delta t \\ 0 & 0 & I - \frac{1}{2} S\left(\underline{\widetilde{m_\omega}}(t) \right) \Delta t \end{bmatrix} \tag{17}$$

where I is the identity matrix, and $Q = \mathrm{diag}\left(0, \sigma_a^2 I, \sigma_\omega^2 I\right)$ is composed of the sensor noise variances (σ_a^2 and σ_ω^2 for respectively the accelerometer and rate gyroscope, where both are assumed isotropic).

For notational convenience, we set $t \leftarrow t + \Delta t$ henceforth. After each prediction step, the reference attitude and state are adjusted as follows, to generate the post-prediction values, denoted with the subscript $p+$

$$\hat{x}_{p_+}(t) = \left(\underline{\hat{p}}_p(t), \underline{\hat{v}}_p(t), 0 \right) \tag{18}$$

$$\underline{\hat{R}_{\mathrm{ref}}}_{p_+}(t) = \underline{\hat{R}_{\mathrm{ref}}}(t) \exp\left(S\left(\underline{\hat{\delta}}_p(t) \right) \right) \tag{19}$$

$$P_{xx,p_+}(t) = T\left(\underline{\hat{\delta}}_p(t) \right) P_{xx,p}\, T\left(\underline{\hat{\delta}}_p(t) \right)^T \tag{20}$$

where, to keep the covariance aligned with $\underline{\hat{R}_{\mathrm{ref}}}$ we use

$$T(\delta) = \mathrm{diag}\left(I, I, \exp\left(-\tfrac{1}{2} S(\delta) \right) \right) \tag{21}$$

If no range measurement is available at time t, we set $\hat{x}(t) = \hat{x}_{p_+}(t)$, and $P_{xx}(t) = P_{xx,p_+}(t)$. If, instead, an ultra-wideband measurement $\widetilde{r}_i(t)$ is available from a beacon i, it is used in the standard EKF formalism (see e.g. [22]) as below

$$H(t) = \left[\left(\underline{\hat{p}}(t) - \underline{b}_i \right)^T \; 0 \; 0 \right] \tag{22}$$

$$K(t) = P_{xx,p_+}(t) H(t)^T \left(H(t) P_{xx,p_+}(t) H(t)^T + \sigma_r^2 \right)^{-1} \tag{23}$$

$$\hat{x}_m(t) = \hat{x}_{p_+} + K(t) \left(\widetilde{r}_i(t) - \left\| \underline{\hat{p}}_{p_+}(t) - \underline{b}_i \right\| \right) \tag{24}$$

$$P_{xx,m}(t) = (I - K(t)H(t)) P_{xx,p_+} \tag{25}$$

$$\underline{\hat{R}_{\mathrm{ref}}}_m(t) = \underline{\hat{R}_{\mathrm{ref}}}_{p_+}(t) \tag{26}$$

Notable is that that the reference rotation is unchanged, and in general $\underline{\hat{\delta}}_m(t) \neq 0$. Thus, a final step is required to correct, given by

$$\hat{x}(t) = \left(\underline{\hat{p}}_m(t), \underline{\hat{v}}_m(t), 0 \right) \tag{27}$$

$$\underline{\hat{R}_{\mathrm{ref}}}(t) = \underline{\hat{R}_{\mathrm{ref}}}_m(t) \exp\left(S\left(\underline{\hat{\delta}}_m(t) \right) \right) \tag{28}$$

$$P_{xx}(t) = T\left(\underline{\hat{\delta}}_m(t) \right) P_{xx,m}(t)\, T\left(\underline{\hat{\delta}}_m(t) \right)^T \tag{29}$$

The estimator then proceeds to absorb the next set of IMU measurements.

Notable is that the full orientation is not observable if the vehicle never accelerates horizontally, as in that case $\underline{\hat{R}_{\mathrm{ref}}}(t)^{-1} \underline{\widetilde{m_a}}(t)$ is parallel to gravity, so that information about the attitude component about gravity does not integrate to the position states through (16).

EXPERIMENTAL VALIDATION

The efficacy of the estimator from the previous section is established in experiment. In the experiment a UAV follows commanded trajectory using only the rate gyroscope, accelerometer, and ultra-wideband ranges for data. All computations for control are done on the UAV itself, on a low-cost microcontroller running at 500Hz.

Simultaneously, a motion capture system is used to record the position of the vehicle. This is not used in closed-loop, but is instead stored as ground-truth, for comparison with the estimator output. Specifically, we use a Crazyflie 2.0 quadcopter, as shown in Fig. 2. Notable is the small size of the vehicle, making its dynamics hard to model, especially as it is greatly influenced by external disturbances.

FIGURE 2. THE QUADCOPTER USED IN THE EXPERIMENTS.

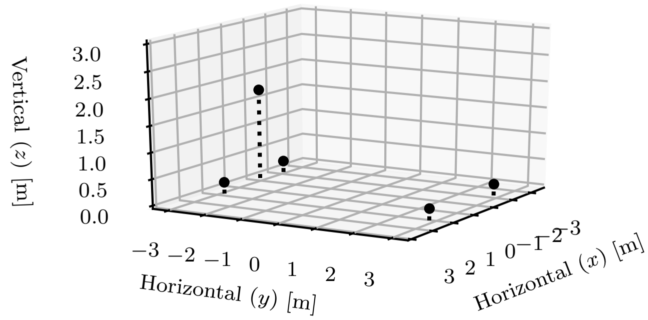

FIGURE 3. BEACON LOCATIONS IN THE EXPERIMENTS.

Sensor characterization

The UAV's inertial measurement unit returns accelerometer and rate gyroscope data at 500Hz. The sensors' associated noise standard deviations σ_a and σ_ω are estimated from in-flight data as below. Note that, due to in-flight vibrations, the sensors show markedly higher noise levels than when stationary. The ultra-wideband ranging noise was characterized from static tests.

$$\sigma_a = 5\,\mathrm{m\,s^{-2}} \tag{30}$$

$$\sigma_\omega = 0.1\,\mathrm{rad\,s^{-1}} \tag{31}$$

$$\sigma_r = 0.5\mathrm{m} \tag{32}$$

The ultra-wideband ranging system measures a distance to a beacon at approximately 100Hz, but does so irregularly. This irregularity is due to failure in transmission of at least one of the four radio messages that make up a ranging communication.

Experimental system setup

Experiments were conducted in the UC Berkeley HiPeRLab indoor experimental flight space. Five radio beacons were used, with four placed near the ground and the fifth mounted against a wall at a height of approximately 1.7m. The beacon positions were as follows, where the inertial z-axis points vertically upwards (this is also visualized in Fig. 3):

$$\underline{b}_1 = (-1.91, 2.98, 0.22)\,\mathrm{m} \tag{33}$$

$$\underline{b}_2 = (1.35, 3.00, 0.22)\,\mathrm{m} \tag{34}$$

$$\underline{b}_3 = (1.12, -2.71, 0.22)\,\mathrm{m} \tag{35}$$

$$\underline{b}_4 = (-1.88, -2.88, 0.22)\,\mathrm{m} \tag{36}$$

$$\underline{b}_5 = (-0.94, -2.98, 1.73)\,\mathrm{m} \tag{37}$$

The vehicle is controlled using the output from the estimator. All control and estimation computation is run on the vehicle's microcontroller at 500Hz. The control algorithm used is described in [23].

Results

Two representative experiments are presented. In the first, the vehicle was commanded to hold a constant position in hover, while for the second the the vehicle was commanded to fly a 1m radius circle at a translational velocity of $0.5\,\mathrm{m\,s^{-1}}$. The position of the vehicle when hovering is shown in Fig. 4, where a flight lasting 60 seconds is shown. The position tracking error in hover are relatively large, on the order of 1m. However, the estimation error in position is much smaller – this suggests that the closed-loop tracking error is not dominated by the vehicle's position estimation error.

An experiment for the circular flight is shown in Figs. 5-7. The experiment begins with the vehicle in flight, and lasts for approximately 95s, ending when the vehicle lands. Fig. 5 shows the vehicle's position tracking performance: notable is that the system has a phase error in tracking the reference position, however the state estimation error is again much smaller than the tracking error.

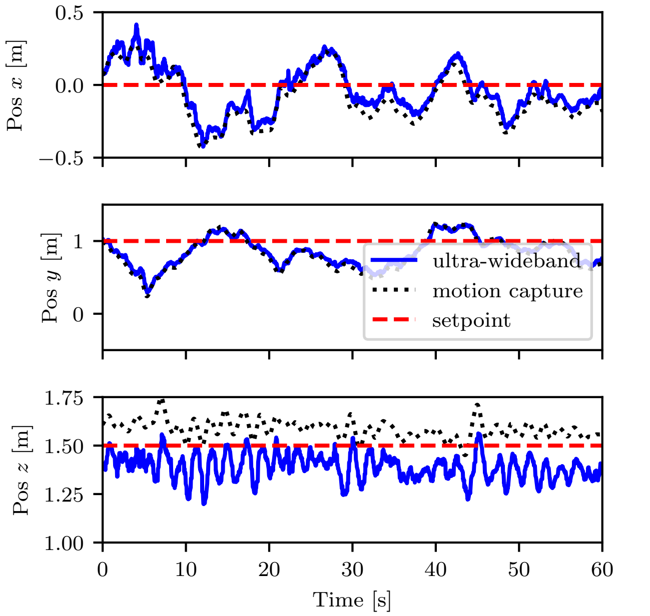

FIGURE 4. POSITION HISTORY OF EXPERIMENTAL FLIGHT FOR HOVER.

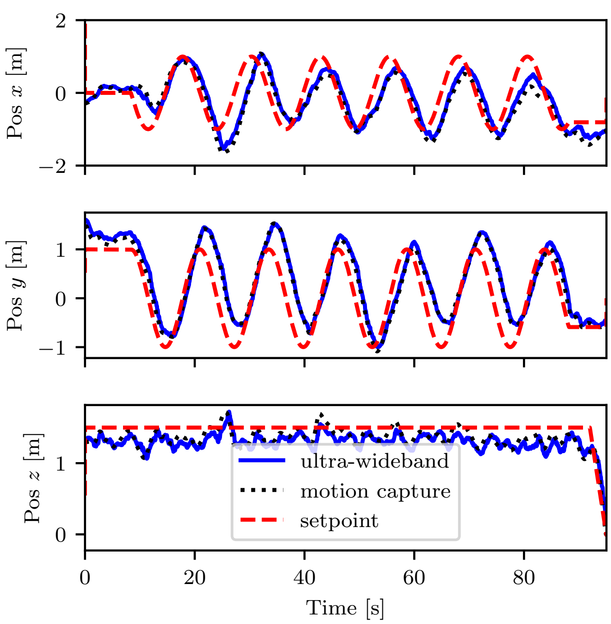

FIGURE 5. POSITION HISTORY OF EXPERIMENTAL FLIGHT FOR CIRCULAR TRAJECTORY.

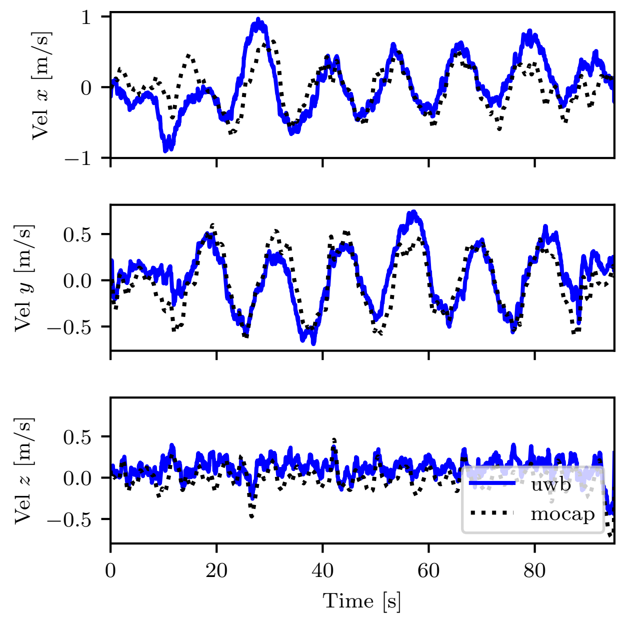

FIGURE 6. POSITION HISTORY OF EXPERIMENTAL FLIGHT CORRESPONDING TO FIG. 5.

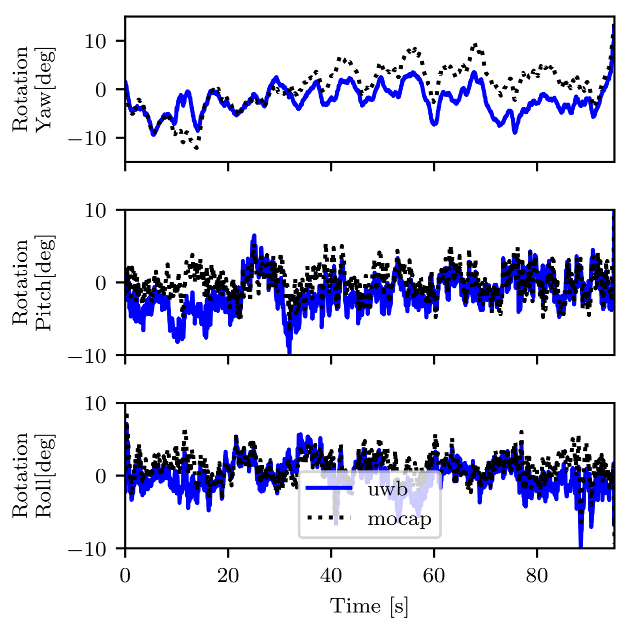

FIGURE 7. ROTATION HISTORY OF EXPERIMENTAL FLIGHT CORRESPONDING TO FIG. 5, SHOWING THE EULER YAW-PITCH-ROLL SEQUENCE.

That suggests that the tracking error is purely a control issue, and most likely due to the use of soft controller gains. As may be expected from the good position estimation, the estimator also performs well when estimating the vehicle's translational velocity, shown in Fig. 6.

The rotational estimate shown in Fig. 7 shows a noticeable difference in performance when estimating the vehicle's rotation about gravity compared to the other two rotational degrees of freedom. The plot shows the attitude broken down into the Euler yaw-pitch-roll sequence, where specifically yaw represents the rotation about gravity. As, during typical operations, the accelerometer measurement is mostly parallel to gravity, this is the degree of freedom that is least strongly observed in flight. This is due to the attitude only being observable through the coupling in the dynamics equation (17), through the term $S\big(\underline{\hat{R}_{\mathrm{ref}}}(t)^{-1}\underline{\widetilde{m_a}}(t)\big)$. Nonetheless, the estimator succeeds in estimating the vehicle's full orientation.

CONCLUSION

We have developed a robust and flexible state estimator for UAVs, relying on the UAV's accelerometer, and rate gyroscope, and using distance measurements from the UAV to ultra-wideband beacons in the environment. The estimator is based on the extended Kalman filter, using the attitude reset steps of [15] to encode the attitude in a statistically correct way. A notable property of the derived estimator is that it requires no knowledge of the vehicle's dynamic properties (such as mass, mass moment of inertia, drag properties, etc). This means that the estimator may be especially useful in applications where these parameters are difficult to estimate, such as when carrying loads. Furthermore, no assumptions were needed about the environment (such as lack of wind). The estimator's performance was validated in experiments.

ACKNOWLEDGMENT

This research was supported by the Department of Mechanical Engineering, UC Berkeley. Experimental results used a codebase to which many people have contributed, a full list is available at http://hiperlab.berkeley.edu/members/.

REFERENCES

[1] How, J., Bethke, B., Frank, A., Dale, D., and Vian, J., 2008. "Real-time indoor autonomous vehicle test environment". IEEE Control Systems Magazine, 28(2), April, pp. 51–64.

[2] Michael, N., Mellinger, D., Lindsey, Q., and Kumar, V., 2010. "The GRASP multiple micro-UAV testbed". IEEE Robotics Automation Magazine, 17(3), September, pp. 56–65.

[3] Lupashin, S., Hehn, M., Mueller, M., Schoellig, A. P., Sherback, M., and D'Andrea, R., 2014. "A platform for aerial robotics research and demonstration: The Flying Machine Arena". Mechatronics, 24(1), pp. 41 – 54.

[4] Preiss, J. A., Honig, W., Sukhatme, G. S., and Ayanian, N., 2017. "Crazyswarm: A large nano-quadcopter swarm". In Robotics and Automation (ICRA), 2017 IEEE International Conference on, IEEE, pp. 3299–3304.

[5] Cadena, C., Carlone, L., Carrillo, H., Latif, Y., Scaramuzza, D., Neira, J., Reid, I., and Leonard, J. J., 2016. "Past, present, and future of simultaneous localization and mapping: Toward the robust-perception age". IEEE Transactions on Robotics, 32(6), pp. 1309–1332.

[6] Meier, L., Tanskanen, P., Heng, L., Lee, G., Fraundorfer, F., and Pollefeys, M., 2012. "PIXHAWK: A micro aerial vehicle design for autonomous flight using onboard computer vision". Autonomous Robots, 33(1-2), pp. 21–39.

[7] Schauwecker, K., and Zell, A., 2013. "On-board dual-stereo-vision for autonomous quadrotor navigation". In International Conference on Unmanned Aircraft Systems (ICUAS), IEEE, pp. 333–342.

[8] Weiss, S., Achtelik, M. W., Lynen, S., Achtelik, M. C., Kneip, L., Chli, M., and Siegwart, R., 2013. "Monocular vision for long-term micro aerial vehicle state estimation: A compendium". Journal of Field Robotics, 30(5), pp. 803–831.

[9] Shen, S., Mulgaonkar, Y., Michael, N., and Kumar, V., 2013. "Vision-based state estimation and trajectory control towards high-speed flight with a quadrotor.". In Robotics: Science and Systems.

[10] Loianno, G., Brunner, C., McGrath, G., and Kumar, V., 2017. "Estimation, control, and planning for aggressive flight with a small quadrotor with a single camera and IMU". IEEE Robotics and Automation Letters, 2(2), pp. 404–411.

[11] Gezici, S., Tian, Z., Giannakis, G., Kobayashi, H., Molisch, A., Poor, H., and Sahinoglu, Z., 2005. "Localization via ultra-wideband radios: a look at positioning aspects for future sensor networks". IEEE Signal Processing Magazine, 22(4), pp. 70–84.

[12] Mahfouz, M., Zhang, C., Merkl, B., Kuhn, M., and Fathy, A., 2008. "Investigation of high-accuracy indoor 3-D positioning using UWB technology". IEEE Transactions on Microwave Theory and Techniques, 56(6), pp. 1316–1330.

[13] Prorok, A., Arfire, A., Bahr, A., Farserotu, J. R., and

Martinoli, A., 2010. “Indoor navigation research with the Khepera III mobile robot: An experimental baseline with a case-study on ultra-wideband positioning”. In International Conference on Indoor Positioning and Indoor Navigation (IPIN), IEEE, pp. 1–9.

[14] Mueller, M., Hamer, M., and D’Andrea, R., 2015. “Fusing ultra-wideband range measurements with accelerometers and rate gyroscopes for quadrocopter state estimation”. In IEEE International Conference on Robotics and Automation (ICRA), IEEE.

[15] Mueller, M., Hehn, M., and D’Andrea, R., 2016. “Covariance correction step for Kalman filtering with an attitude”. Journal of Guidance, Control, and Dynamics, pp. 1–7.

[16] Zipfel, P. H., 2007. Modeling and Simulation of Aerospace Vehicle Dynamics Second Edition. AIAA.

[17] Martin, P., and Salaun, E., 2010. “The true role of accelerometer feedback in quadrotor control”. In IEEE International Conference on Robotics and Automation (ICRA), IEEE, pp. 1623–1629.

[18] Mahony, R., Kumar, V., and Corke, P., 2012. “Aerial vehicles: Modeling, estimation, and control of quadrotor”. IEEE Robotics & Automation Magazine, 19(3), pp. 20–32.

[19] Leishman, R., Macdonald, J., Beard, R., and McLain, T., 2014. “Quadrotors and accelerometers: State estimation with an improved dynamic model”. Control Systems, IEEE, 34(1), pp. 28–41.

[20] Craig, W., and Paley, D. A., 2017. “Geometric control of quadrotor attitude in wind with flow sensing and thrust constraints”. In ASME 2017 Dynamic Systems and Control Conference, American Society of Mechanical Engineers, pp. V001T02A005–V001T02A005.

[21] Shuster, M. D., 1993. “A survey of attitude representations”. Journal of the Astronautical Sciences, 41(4), pp. 439–517.

[22] Simon, D., 2006. Optimal state estimation: Kalman, H infinity, and nonlinear approaches. John Wiley & Sons.

[23] Mueller, M., 2018. “Multicopter attitude control for recovery from large disturbances”. ArXiv e-prints: 1802.09143, Feb.